Modelling start-up injection of CO_2 into highly-depleted gas fields

Andrea Sacconi and Haroun Mahgerefteh*
Department of Chemical Engineering, University College London, London WC1E 7JE, UK

Abstract

The development and verification of a homogeneous relaxation model for simulating the highly transient flow phenomena taking place during the start-up injection of CO_2 into deep highly depleted gas fields is presented. The constituent mass, momentum, and energy conservation equations, incorporating a relaxation time to account for non-equilibrium effects, are solved numerically for single and two-phase flows along the steel lined injection well leading to the storage reservoir. Wall friction, gravitational field effects and heat transfer between the expanding fluid and the outer well layers are taken into account as source terms in the conservation equations. At the well inlet, the opening of the upstream flow regulator valve is modelled as an isenthalpic expansion process; whilst at the well outlet, a formation-specific pressure-mass flow rate correlation is adopted to characterise the storage site injectivity. The testing of the model is based on its application to CO_2 injection into the depleted Golden Eye Reservoir in the North Sea for which the required design and operational data are publically available. Three injection scenarios involving a rapid, medium and slow linear ramping up of the injected CO_2 flow rate to the peak nominal value of 33.5 kg/s are simulated. In each case, the predicted pressure and temperature transients at the top and bottom of the well are employed to ascertain the risks of well-bore thermal shocking, and interstitial ice or CO_2 hydrate formation leading to its blockage due to the rapid expansion cooling of the CO_2. The results demonstrate the efficacy of the proposed model as a tool for the development of optimal injection strategies and best-practice guidelines for the minimisation of the risks associated with the start-up injection of CO_2 into depleted gas fields.

Keywords: Global warming, Carbon Capture and Storage, CO2 injection, Transient flow modelling

*corresponding author h.mahgerefteh@ucl.ac.uk

1. Introduction

According to the IEA Energy Technology Perspective [1], Carbon Capture and Sequestration (CCS) is expected to play a key role in moving the CO_2 emitting energy intensive industries, such as iron and steel, cement and oil refineries onto a pathway consistent with limiting the increase in global average temperatures to well below 2°C above pre-industrial levels as agreed at the Paris Climate Conference in 2015. The safe and cost effective storage of the enormous amounts of CO_2 captured from these sources is an essential element of CCS and therefore of fundamental importance in ensuring its success. Highly-depleted gas fields offer excellent potential for the permanent storage of the captured CO_2 [2]. In the case of the UK for example, the Southern North Sea and the East Irish Sea depleted gas reservoirs provide almost 95% of the storage capacity required to meet UK's CO_2 reduction commitments for the period 2020-2050 [3].

As compared to saline aquifers, depleted gas fields are better characterized given the availability of geological data, such as pressure, porosity and permeability, derived from years of gas production. They have seals that have successfully retained hydrocarbon gas for millions of years, and may offer a shorter route to practical implementation for early Carbon Capture and Storage (CCS) projects [4].

The UK has completed three large FEED study projects for offshore CO_2 storage at Hewett, Golden Eye and Endurance sites [5]. However, CO_2 storage at full industrial scale has only been demonstrated at a small number of sites around the world: Sleipner, In Salah & Snøvit [6], Ordos [7], and the Quest project [8].

In order to boost the confidence of both investors and the public and thus facilitate the full-scale deployment of CCS, it is of paramount importance to guarantee that the storage site will be of high quality and operate in a safe manner.

However, given the low reservoir pressures along with the unique thermodynamic properties of CO_2, the start-up injection of CO_2 into depleted low-pressure gas fields presents significant safety and operational challenges.

The most practical cost-effective option for transporting the captured CO_2 involves the use of sub-sea pipelines with the CO_2 in the dense or liquid phase, i.e. above 75 bar given the lower pressure drop along the pipeline as compared to the gas phase and the larger line pack [9–12]. As the sea temperature will be well below the CO_2 critical temperature (31.1 ^{o}C), the fluid will arrive in the liquid state. Given the much lower wellhead pressure, the uncontrolled injection of the CO_2 into the wellhead will lead to its rapid quasi adiabatic expansion (often referred to as Joule Thomson cooling) into a two-phase mixture leading to temperatures well below zero ^{o}C [13].

In practice, the rapid expansion cooling could pose several operational and safety risks, namely:

- CO_2 hydrate and ice formation following contact of the cold CO_2 with the interstitial water around the wellbore and the formation water in the perforations at the near well zone. The former poses the risk of well blockage, while the latter may severely reduce the reservoir injectivity and ultimately its storage capacity;

- thermal stress shocking of the wellbore casing steel leading to its fracture and the escape of CO_2;

- thermal stress shocking of the reservoir rocks leading to fracture thus changing the reservoir permeability and reducing 'its CO_2 locking' effectiveness;

- superheating of the liquid CO_2 at the wellhead leading to its violent evaporation and over-pressurisation followed by CO_2 backflow into the injection system.

As such, developing appropriate start-up injection strategies where the rate of injection of CO_2 is gradually increased in a controlled manner is of paramount importance for avoiding the above risks. Key to this is the availability of reliable mathematical models for predicting the behaviour of the injected CO_2, in particular its variation of pressure and temperature along the well and ultimately at the point of entry into the depleted reservoir. The alternative is the heating of the CO_2 stream prior to injection, which is highly costly given the significant volumes involved.

Driven by the push to reduce CO_2 emissions along with the economic incentives associated with enhanced natural gas recovery involving CO_2 injection into depleted natural gas reservoirs, several, almost exclusively modelling studies focusing on the associated temperature and pressure transients with various degrees of sophistication have been reported in the open literature. The following is a critical review of the main models. The review does not cover the much simpler case of injection of CO_2 into aquifers [14]. Given the much higher aquifer pressures, the rapid fluid expansion transient phenomenon associated with the injection of CO_2 in depleted gas fields are not expected here and hence irrelevant to the scope of the present work.

Olenbuurg [15] employed the commercially available ToughTOUGH2 module to simulate the radial variation of the reservoir temperature at the bottom of the well for different natural gas reservoir permeabilities and constant injection CO_2 flow rates, reporting a cooling of approximately 20 °C. Goodarzi et al [16] employed a coupled flow, aeromechanical and heat transfer model for the injection and sequestration of CO_2 in Ohio Valley. However their model was limited to simulating the impact on the injection zone and the surrounding formations in order to evaluate the risk of induced fracturing of the storage formation following exposure to the incoming low temperature CO_2 stream.

Linga and Lund [17] developed a sophisticated two-fluid model applied to CO_2 injection wells incorporating the Span–Wagner equation-of-state [18]. However, much the same as Li et al [19], the application of their model was limited to predicting the resulting temperature and pressure profiles following well blowout and during shut in. Temperatures as low as − 48°C were predicted upon blowout concluding that this temperature was not necessarily low enough to cause damage to the steel pipe itself, but likely to pose a hazard due to mechanical stresses that arise due to thermal contraction.

Lu and Connell [20] presented a model to simulate the flow of CO_2 and its mixtures in non-isothermal wells. However their model was based on steady state flow, therefore incapable of dealing with the rapid transients occurring during the start-up injection phase. Paterson et al [21] too developed a steady state flow model in order to predict the bottom hole well pressure following the injection of CO_2 for Enhanced Oil Recovery (EOR).

Lindeberg et al [22] used the Bernoulli's pressure drop equation along with heat transfer and frictional effects to predict injection well temperature profile for the steady state injection of CO_2 for Sleipner CO_2 storage project to show that adiabatic conditions flow conditions along the well could be assumed after a few months even if the injection is regularly stopped for one to two weeks for servicing. Pan et al [23] using the drift flux conceptual model presented analytical solutions for compressible two-phase flow thorough a 1000 m , 0.1m dia. well bore under isothermal and homogenous equilibrium flow conditions accounting for phase slip. Verifying their predictions of the gas phase velocity and drift velocity versus well depth against the results of the commercially numerical wellbore flow simulator T2Well, the authors used their model to evaluate how the bottom hole pressure in a well in which CO_2 is leaking upward responds to the mass flow rate of CO_2–water mixture. Lu and Connell [24] presented a transient flow model based on the homogenous equilibrium where the constituent phases are assumed to be at thermal and mechanical equilibrium coupled with a steady state heat transfer model for the injection of liquid CO_2 into a 560 m deep 0.03m dia. well for a field trial of CO_2 enhanced coal bed methane recovery. Critically important information such as the CO_2 injection rate and its variation with time was not given. The subsequent fluid bottom-hole pressure and temperature data for a period of 3.5 h following the completion of the injection process were simulated. The model was incapable of handling the injection start-up process were the transient variations in the CO_2 temperature and pressure are expected to be most pronounced. Relatively poor agreement between model predictions of the transient temperature data against the recorded data were reported despite significant modifications of the heat transfer model.

Munkejord et al [25] conducted three case studies relating to the transport and injection of CO_2. In the first case study, the authors generated the pressure/enthalpy phase diagram for compression/cooling trajectories for pure CO_2 and 5% CH4 / 95% methane in order to determine the fluid phase arriving at the well head. The second case study dealt with the abandoned Vattenfall CCS demonstration project involving the retrofitting of a post-combustion capture unit to the Nordjyllandsværket coal-fired power plant and transporting the captured CO_2 to an onshore saline aquifer using a 24 km pipeline. The commercial software ,OLGA incorporating a drift flux model by Kjell and Bendiksen [26] was employed to track the well bottom hole pressure/time response following a variable mass flow rate injection loading. Given that CO_2 is injected into a high pressure (213 bar) aquifer, the relatively slow mass flow ramping rate employed, along with CO_2 remaining in the dense phase throughout the injection well, as expected, given the relatively large velocity of sound in the fluid (ca. 1000 m/s), the bottom hole pressure reacted almost instantaneously in response to a change in the feed mass flow rate. In case study 3, the OLGA was employed to simulate the pressure and temperature/time profiles for the depressurisation of a subsea pipeline transporting captured CO_2 from flue gas emitted by the combined heat and power plant at Mongstad into suitable locations on the Norwegian Continental Shelf.

Li et al [27] coupled a steady-state thermo-hydraulic model describing flow of CO_2 in an injection well with a transient model for radial heat conduction in the rock formation surrounding the well. The model enabled the analysis of slow transients in the flow and heat transfer occurring during the temperature equilibration between the well and the formation upon a steady-state injection conditions. The model was validated against real data, showing a good agreement with the bottom hole pressure and temperature measured in a test involving injection of supercritical CO_2. However, due to the underlying assumption of steady-state flow, the model is not suitable for analysis of start-up injection where large temperature variations in the well fluid are induced as a `consequence of the rapid expansion of the CO_2 in the wellhead.

Lund et al [28] employed a heat conduction model based on finite volume method for determining the heat transfer from the well to the casing, annular seal, and rock formation following the injection of CO_2 for EoR applications. Their predictions of the temperature variations at various locations in and around a given well during CO_2 injection

were found to be in relatively good agreement with those based on small scale laboratory experiments. The authors used their model to conclude, as expected, that by replacing cement with an annular sealant material with higher thermal conductivity, the temperature difference across the seal can be significantly reduced thus reducing the risk associated with the thermal shocking of the well.

In a report by Shell [29] (see Section 4), the transient variations of the well head and well bottom pressure and temperature were reported for the injection of CO_2 into the depleted Golden Eye reservoir using OLGA. However no information is publically available describing the detailed development of the above flow model in pipes for the simulation of the more complex start-up injection of CO_2 through a vertical well discharging into the reservoir at different ramping up injection rates.

Based on the above review, it is clear that much of the reported models on CO_2 injection into well bores are based on steady-state flow assumption where the rapid pressure and temperature transients associated with the start-up injection process cannot be handled. The drift-flux flow models dealing with multi-phase flow behaviour usually contain several empirical parameters that must be determined experimentally. They are also notoriously prone to numerical stabilities or singularities at either flow regime transitions or when the liquid volume fraction approaches zero [30]. The use of the sophisticated commercial simulator OLGA, also incorporating drift-flux flow complicates the model validation since little information is publically available regarding its details.

In this paper the development and verification of a mathematical model for simulating the transient flow phenomena taking place during the start-up injection of CO_2 into highly depleted gas fields is presented. The formulation is based on a Homogeneous Relaxation Model (HRM), where mass, momentum, and energy conservation equations are considered for single or two-phase flows. The model accounts for phase and flow dependent fluid/wall friction and heat transfer, variable well cross sectional area as well as deviation of the well from the vertical.

At the well inlet, the opening of the upstream flow regulator valve is modelled as an isenthalpic expansion process; whilst at the well outlet, a pre-defined site-characteristic pressure-mass flow rate correlation is used to simulate the migration of the CO_2 into the geological substrate. The developed model is next employed to perform a detailed sensitivity analysis of the most important parameters affecting the CO_2 flow behaviour, including the upstream temperature, pressure and time variant mass flow rate; the latter being representative of the feed pressure ramping up process. These investigations are intended to demonstrate the efficacy of the injection model presented as a practical tool for the development of optimal injection strategies and best-practice guidelines for minimising the risks associated with the start-up injection of CO_2 into depleted gas fields.

2. Model formulation

2.1 Wells and injection scenarios

Wells are an essential component of any CO_2 storage project. They are the only way by which CO_2 can be discharged into underground reservoirs in the timeframes required. It is important to recognise that the injected CO_2 is not stored in the wells. The well represents the transportation route through which the CO_2 will be released into reservoirs and then remain safely trapped. Wells are drilled for a range of purposes such as exploration, appraisal, production, injection or monitoring. Well objectives strongly influence its design, depth, size and cost. The information gathered from existing wells drilled and used by oil and gas operators proves to be very useful in characterising the subsurface geology of a site [5]. A schematic of typical well for the injection of CO_2 into a depleted gas field is represented in Figure 1. The well is composed of various layers and surrounded by a formation, whose composition varies from site to site. Wells have to be carefully analysed in order to assess their suitability for CO_2 injection in depleted oil and gas fields [31].

Before the steady injection of CO_2 into the reservoir can be started, it is necessary to perform time-dependent operations to estimate important reservoir properties, e.g. permeability and pressure. Such operations include start-up, shut-in and emergency shut-down, which prove to be critical in the overall design of the well [9]. Even after steady injection conditions are reached, the well may be shut in and started up for maintenance of the upstream transportation

system or other routine checks. It is therefore of paramount importance to be able to predict the behaviour of the CO_2, in terms of pressure and temperature, particularly at the top and bottom of the well in order to identify and quantify potential risks.

2.2 Fluid dynamics

The following gives an account of the extension of our previously developed Homogeneous Relaxation Model ((HRM) [32,33]) employed for the simulation of the time-dependent flow of CO_2 injected into the well. The system of four partial differential equations for the CO_2 liquid/gas mixture, to be solved in the well tubing can be written in the well-known conservative form as follows:

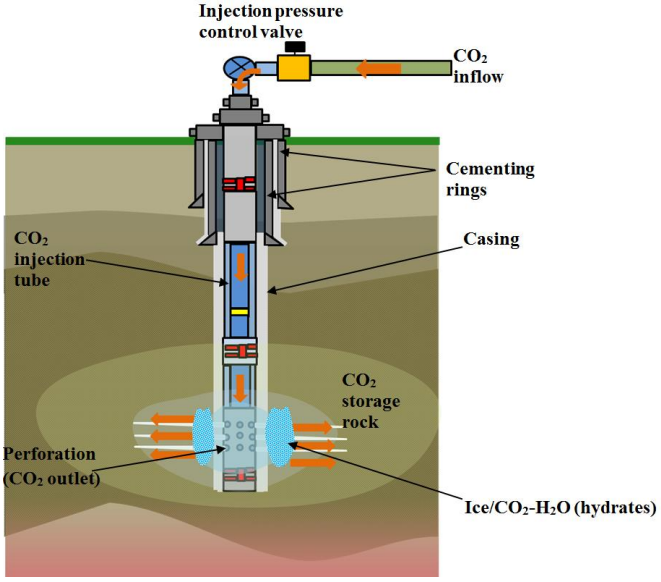

Figure 1: Schematic representation of a deep well CO_2 injection and storage facility

$$\frac{\partial}{\partial t}\boldsymbol{U} + \frac{\partial}{\partial z}\boldsymbol{F}(\boldsymbol{U}) = \boldsymbol{S_1} + \boldsymbol{S_2} \tag{1}$$

Where, we define;

$$\boldsymbol{U} = \begin{pmatrix} \rho A \\ \rho u A \\ \rho E A \\ A \end{pmatrix}, \quad \boldsymbol{F}(\boldsymbol{U}) = \begin{pmatrix} \rho u A \\ \rho u^2 A + AP \\ \rho u H A \\ 0 \end{pmatrix}, \quad \boldsymbol{S_1} = \begin{pmatrix} 0 \\ P\dfrac{\partial A}{\partial z} \\ 0 \\ 0 \end{pmatrix}, \quad \boldsymbol{S_2} = \begin{pmatrix} 0 \\ A(F + \rho\beta g) \\ A(Fu + \rho u\beta g + Q) \\ 0 \end{pmatrix} \tag{2}$$

In the above, the first three equations correspond to mass, momentum, and energy conservation respectively. The fourth equation accounts for the fact that the well bore cross-sectional area A at any location along the well does not change with time, but may vary along the well. u and ρ are the mixture velocity and density respectively. P is the mixture pressure, while E and H represent the specific total energy and total enthalpy of the fluid, respectively. These are in turn are defined as:

$$E = e + \frac{1}{2}u^2 \tag{3}$$

$$H = E + \frac{P}{\rho} \tag{4}$$

where, e is the specific internal energy. z denotes the axial coordinate, t the time, F the viscous friction force, Q the heat flux, and g the gravitational acceleration. Given the rapid transients during decompression, phase slip is ignored. However, non-equilibrium liquid-vapour transition is accounted for by a relaxation to thermodynamic equilibrium through the following equation [34]:

$$\frac{\partial x}{\partial t} + u\frac{\partial x}{\partial z} = \frac{x_e - x}{\theta} \tag{5}$$

where, x is the mixture vapour quality and θ is a relaxation time accounting for the delay in the phase change transition. The mixture density ρ is defined as:

$$\frac{1}{\rho} = \frac{x}{\rho_{sv}(P)} + \frac{1-x}{\rho_{ml}(P, e_{ml})} \tag{6}$$

while the mixture internal energy is defined as:

$$e = xe_{sv}(P) + (1-x)e_{ml} \tag{7}$$

Where, the subscripts sv and ml refer to the saturated vapour and meta-sTable (super-heated) liquid phases respectively.

The various source terms appearing on the right-hand side of equation (2) are described next.

The frictional loss, F can be expressed as:

$$F = -f_w \frac{\rho u^2}{D_p} \tag{8}$$

where, f_w is the Fanning friction factor, calculated using Chen's correlation [35], and D_p is the internal diameter of the pipe.

The gravitational term is given by

$$\beta(z) = \rho g \sin\theta \tag{9}$$

where, θ is the well deviation from the vertical. In practice, a well is often not drilled in the perfectly vertical direction. Deviations may be caused by geological conditions, specifics of the drilling technology and the process conditions [36,37]. The well deviation and consequently the corresponding gravitational term in equation (9) is usually expressed through two different quantities: True Vertical Depth (TVD) and Measured Depth (MD). The former denotes the vertical distance from the wellhead to a point in the well path. Such quantity is calculated from directional survey data. MD on the other hand denotes the actual length of the well, and it is always greater than the corresponding TVD, given the wellbore deviation from the vertical.

In equation (2) the source term, Q accounts for the heat exchange between the fluid and the well wall. The corresponding heat transfer coefficient, η is calculated using the well-known Dittus-Boelter correlation [38]:

$$\eta = 0.023\, Re^{0.8} Pr^{0.4} \frac{k}{D_p} \tag{10}$$

where, k, Re and Pr are the thermal conductivity, Reynolds number and Prandtl number for the fluid respectively. The heat exchange between the fluid and the well wall is given by:

$$Q = \frac{4}{D_p}\eta(T_w - T) \tag{11}$$

where, T_w and T are the fluid and wall temperatures respectively. Note that $T_w = T_w(z,t)$, i.e. T_w is not assumed constant, but variable with time and space. The transient heat conduction in the coordinate r (the radial direction from the axis of the well towards the well layers and the formation surrounding the well) is solved using the following equation [28]:

$$\rho(r)c_p(r)\frac{\partial}{\partial t}T(r,t) = \frac{1}{r}\frac{\partial}{\partial r}\left(r\kappa(r)\frac{\partial}{\partial r}T(r,t)\right) \tag{12}$$

where, c_p and κ respectively represent heat capacity and heat conductivity at the radial coordinate r.

In order to close the Homogeneous Relaxation Model system of equations (Equation (1)&(2)), the pertinent thermodynamic properties for vapour and liquid phases are calculated with the aid of the Peng–Robinson Equation of State (EoS) [39]. It should be noted that while other more accurate EoS exist for pure CO_2 exist e.g. [18,40], the computational workload required to use them in conjunction with our Homogeneous Relaxation Model is currently prohibitive. The PR equation of state is given by

$$P = \frac{R}{v-b} - \frac{c\delta}{v^2 + 2bv + -b^2} \tag{13}$$

where, c, b and δ are respectively given by:

$$c = 0.45724\ \frac{(RT_c)^2}{P_c} \tag{14}$$

$$b = 0.0778\ \frac{RT_c}{P_c} \tag{15}$$

$$\delta = \left[1 + \ (0.37464 + 1.54226\omega - 0.2699\omega^2)\left(1 - \sqrt{\frac{T}{T_c}}\right)\right] \tag{16}$$

where, P_c, T_c and ω are respectively the critical pressure, the critical temperature and the acentric factor for CO_2.

From equation (13), the internal energy may be calculated using the identity [41]:

$$e - \ e_{ig} = \int_{-\infty}^{v}\left[T\left(\frac{\partial P}{\partial T}\right)_v - P\right]dv \tag{17}$$

where, the subscript, ig refers to ideal gas. The mixture speed of sound, c is defined through the relation:

$$\frac{1}{\rho c^2} = \frac{x}{\rho_v c_v^2} + \frac{1-x}{\rho_l c_l^2} \tag{18}$$

3. Numerical solution method

As the HRM system of equations (2) cannot be solved analytically, a suitable numerical method has been employed within the Finite Volume framework. More specifically, in order to accurately capture the rich flow dynamics, the AUSM+-up Flux Vector Splitting scheme [42] has been applied to the fluid problem. The solution domain is first divided into N cells and integrated over the i-th computational cell $\left[z_{i-\frac{1}{2}}, z_{i+\frac{1}{2}}\right], i = 1, \dots, N$, to yield the semi-discrete formulation:

$$\frac{d\boldsymbol{U}_i}{dt} = -\frac{1}{\Delta x}\left(\boldsymbol{F}_{i+\frac{1}{2}} - \boldsymbol{F}_{i-\frac{1}{2}}\right) + \boldsymbol{S}_{1,i} + \boldsymbol{S}_{2,i} \tag{19}$$

where $i + \frac{1}{2}$ denotes the interface between cells i and $i + 1$, at which the inter-cell flux $\boldsymbol{F}_{i+\frac{1}{2}}$ has to be computed. Following the standard AUSM method [42], the conservative flux vector is split into convective and pressure fluxes:

$$\boldsymbol{F}_{i+\frac{1}{2}} = \boldsymbol{f}^c{}_{i+\frac{1}{2}} + \boldsymbol{f}^p{}_{i+\frac{1}{2}} \tag{20}$$

where

$$\boldsymbol{f}^c{}_{i+\frac{1}{2}} = \begin{pmatrix} \rho u A \\ \rho u^2 A \\ \rho u H A \\ 0 \end{pmatrix}_{i+\frac{1}{2}}, \quad \boldsymbol{f}^p{}_{i+\frac{1}{2}} = \begin{pmatrix} 0 \\ AP \\ 0 \\ 0 \end{pmatrix}_{i+\frac{1}{2}} \tag{21}$$

3.1 Convective flux discretisation

From equation (21) the convective flux can be written explicitly as

$$\boldsymbol{f}^c = \dot{m}\begin{pmatrix}1\\ u\\ H\\ 0\end{pmatrix} = \dot{m}\boldsymbol{\Psi} \tag{22}$$

where, $\dot{m}$ is the area-weighted mass flux:

$$\dot{m} = \rho u A \tag{23}$$

The numerical flux at cell interface $i + \frac{1}{2}$ is then defined as:

$$\boldsymbol{f}^c{}_{i+\frac{1}{2}} = \dot{m}^*\boldsymbol{\Psi}^* = \dot{m}^*\frac{1}{2}(\boldsymbol{\Psi}_i + \boldsymbol{\Psi}_{i+1}) + \frac{1}{2}|\dot{m}^*|(\boldsymbol{\Psi}_i - \boldsymbol{\Psi}_{i+1}) \tag{24}$$

In order to express $\dot{m}$, the interface speed of sound $a_{i+\frac{1}{2}}$ and the left and right Mach numbers are defined as follows:

$$a_{i+\frac{1}{2}} = \frac{a_i + a_{i+1}}{2}, \qquad M_i = \frac{u_i}{a_{i+\frac{1}{2}}}, \qquad M_{i+1} = \frac{u_{i+1}}{a_{i+\frac{1}{2}}} \tag{25}$$

The interface Mach number is next defined as:

$$\widetilde{M}_{i+\frac{1}{2}} = \mathcal{M}_4^+(M_i) + \mathcal{M}_4^-(M_{i+1}) \tag{26}$$

where $\mathcal{M}^+$ and $\mathcal{M}^-$ are the polynomials introduced by Liou [40] and the subscripts indicating the order of the polynomial used:

$$\mathcal{M}_1^{\pm} = \frac{1}{2}(M \pm |M|) \tag{27}$$

$$\mathcal{M}_2^{\pm} = \pm\frac{1}{4}(M \pm 1)^2 \tag{28}$$

$$\mathcal{M}_4^{\pm} = \begin{cases}\dfrac{\mathcal{M}_1^{\pm}}{M}, & \text{where } |M| \geq 1\\ \pm\,\mathcal{M}_1^{\pm}\left(1 \mp 16B\mathcal{M}_2^{\mp}\right)\end{cases} \tag{29}$$

with $B = \frac{1}{8}$.

In order to approximate numerically the area-weighted mass flux introduced in equation (23), we define:

$$\dot{m}^* = a_{i+\frac{1}{2}}\left[\frac{(\rho A)_i}{2}\left(M_{i+\frac{1}{2}} + \left|M_{i+\frac{1}{2}}\right|\right) + \frac{(\rho A)_{i+1}}{2}\left(M_{i+\frac{1}{2}} - \left|M_{i+\frac{1}{2}}\right|\right)\right] \tag{30}$$

where, $M_{i+\frac{1}{2}} = \widetilde{M}_{i+\frac{1}{2}}$. However, at low Mach numbers this approximation approaches a central difference scheme and can suffer from odd-even decoupling [43]. In order to avoid poor numerical solutions, a velocity-based dissipation is add to $\widetilde{M}_{i+\frac{1}{2}}$:

$$M_{i+\frac{1}{2}} = \widetilde{M}_{i+\frac{1}{2}} - K_p \max(1 - \bar{M}^2, 0)\frac{P_{i+1} - P_i}{\bar{\rho}\bar{a}^2} \tag{31}$$

where, $\bar{M}$, $\bar{\rho}$ and $\bar{a}$ represent the arithmetic averages of the values attained by Mach number, density and speed of sound in cells i and $i + 1$. K_p is a constant, which is set to unity in this study.

While the above scheme has proven to be remarkably robust, in order to avoid instabilities at discontinuities in the cross-sectional area, given its greater degree of dissipation at low Mach numbers, we follow [44] to replace $\widetilde{M}_{i+\frac{1}{2}}$ in Eq. (26) with

$$\widetilde{M}_{i+\frac{1}{2}} = \mathcal{M}_1^+(M_i) + \mathcal{M}_1^-(M_{i+1}) \tag{32}$$

3.2 Pressure flux discretisation

In equation (21) pressure flux $\boldsymbol{f}^p{}_{i+\frac{1}{2}}$ was introduced. According to the AUSM+ splitting, its non-zero element is defined as:

$$(AP)_{i+\frac{1}{2}} = A_{i+\frac{1}{2}}(\mathcal{P}_5^+(M_i)\cdot P_i + \mathcal{P}_5^-(M_{i+1})\cdot P_{i+1}) \tag{33}$$

where the polynomials $\mathcal{P}_5^{\pm}$ are those introduced in Liou [40] and the subscript indicates the order of the polynomial used:

$$\mathcal{P}_5^{\pm} = \begin{cases} \dfrac{\mathcal{M}_1^{\pm}}{M}, & \text{where } |M| \geq 1 \\ \pm\, \mathcal{M}_2^{\pm}\left(2 \mp M - 16CM\mathcal{M}_2^{\mp}\right) \end{cases} \tag{34}$$

with $C = \frac{3}{16}$.

In equation (33) $\mathrm{A}_{\mathrm{i}+\frac{1}{2}}$ can attain two different values in the two cells separated by the interface $\mathrm{i}+\frac{1}{2}$. Specifically, for the i-th cell, $\mathrm{A}_{\mathrm{i}+\frac{1}{2}}$ takes the value of the area on the left of the interface, i.e. $\mathrm{A}_{\mathrm{i}+\frac{1}{2},\mathrm{i}}$, while in the case of the (i + 1)-th cell, $\mathrm{A}_{\mathrm{i}+\frac{1}{2}}$ is set to the value on the right of the interface, i.e. $\mathrm{A}_{\mathrm{i}+\frac{1}{2},\mathrm{i}+1}$. This strategy allows discontinuous variations in the area at the interface $\mathrm{i}+\frac{1}{2}$.

Finally, a dissipation term is added to $\mathrm{P}_{\mathrm{i}+\frac{1}{2}}$. The form of the dissipation term developed by Liou [40] has been widely used for both single and two-phase flows [45,46] and is given by:

$$P_{i+\frac{1}{2}} = \mathcal{P}_5^{+}(M_i)(P)_i + \mathcal{P}_5^{-}(M_{i+1})(P)_{i+1} - K_u\mathcal{P}_5^{+}(M_i)\mathcal{P}_5^{-}(M_{i+1})(\rho_i + \rho_{i+1})a_{i+\frac{1}{2}}(u_{i+1} - u_i) \tag{35}$$

where, K_u is constant and set to unity. However, in order to maintain stability at discontinuities in the cross-sectional area, equation (35) is modified to incorporate a dependency on the cross-sectional area:

$$P_{i+\frac{1}{2}} = \mathcal{P}_5^{+}(M_i)(P)_i + \mathcal{P}_5^{-}(M_{i+1})(P)_{i+1} - K_u\mathcal{P}_5^{+}(M_i)\mathcal{P}_5^{-}(M_{i+1})(\rho_i + \rho_{i+1})a_{i+\frac{1}{2}}\frac{A_{i+\frac{1}{2},i+1}u_{i+1} - A_{i+\frac{1}{2},i}u_i}{\max\left(A_{i+\frac{1}{2},i+1}, A_{i+\frac{1}{2},i}\right)} \tag{36}$$

3.3 Non-conservative fluxes

The discretisation of the source term, $\boldsymbol{S_1}$ containing the non-conservative derivative requires special attention to ensure numerical stability. In particular we take:

$$\boldsymbol{S}_{1,i} = \frac{P_i}{\Delta \mathrm{z}}\begin{pmatrix} 0 \\ \Delta_i A \\ 0 \\ 0 \end{pmatrix} \tag{37}$$

By analogy with the non-conservative terms in the multi-fluid equations studied by [47], the non-zero term in equation (37) is discretised as follows:

$$\Delta_i A = A_{i+\frac{1}{2},i} - A_{i-\frac{1}{2},i} \tag{38}$$

where the areas at the interfaces are taken from within the cell. Analogously, it is easy to show that the non-disturbance relation discussed by [47] holds also here, i.e. under steady conditions with $u = 0$ and $P = const$ the discretisation preserves the relation:

$$\frac{\partial(AP)}{\partial z} = P\frac{\partial A}{\partial z} \tag{39}$$

3.4 Temporal discretisation

Equation (19) is integrated over the time interval, Δt using an Explicit Euler method. The vapour quality relaxation equation (5) is then solved as shown in [32].

3.5 Boundary conditions

So far the methodology for updating the cell value $\boldsymbol{U}_i$ has been presented assuming that the neighbouring cell values $\boldsymbol{U}_{i-1}$ and $\boldsymbol{U}_{i+1}$ in order to compute the inter-cell fluxes $\boldsymbol{F}_{i+\frac{1}{2}}$ and $\boldsymbol{F}_{i-\frac{1}{2}}$ are available. Given that in practice a finite set of grid cells covering the computational domain exists, the first and last cells will not have the required neighbouring information. In order to close the flow equations, the relevant boundary conditions are imposed by adding a ghost cell at either end of the well [48]. All the thermodynamic properties in the ghost cells are set at the beginning of each time step according to the appropriate boundary condition. It is noted that the boundary conditions explicitly depend on time, given the unsteady nature of the start-up injection of CO_2.

The following gives a detailed account of both inflow and outflow boundary conditions.

The mass flow rate at the well injector is determined by the well operator according to the upstream conditions of the transportation system that supplies CO_2 to the storage site. The CO_2 arrives at a certain pressure and temperature and undergoes an isenthalpic process through a choke valve. The implementation of the inflow boundary condition is represented in Figure 2, where the temporal evolution of the thermodynamic variables in the ghost cell at the top of the computational domain is analysed. At every time step, t, a system of three nonlinear equations represented by the following three conditions using the Matlab DASSL solver are resolved:

1. the pressure in the ghost cell will equate the pressure in the first computational cell at time $t - \Delta t$;

2. the CO_2 feed stream, arriving with predefined upstream pressure and temperature, undergoes an isenthalpic process. The enthalpy in the ghost cell will therefore equate the enthalpy of the feed stream;

3. the mass flow rate, as imposed by the well operator, is preserved.

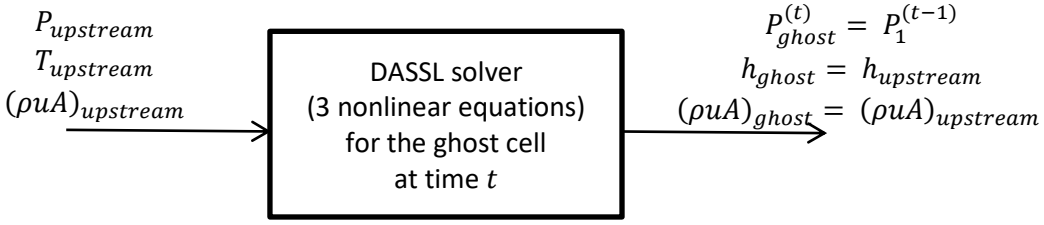

Figure 2: Schematic representation of the isenthalpic inflow condition in the ghost cell at the top of the computational domain.

Note that two of the above conditions carry information coming from outside the domain (namely, the conservation of enthalpy and the mass flow rate prescribed by the well operator), while only one piece of information is provided from the interior of the domain. This is in line with the analysis of time-dependent boundary conditions for subsonic inflows [49,50].

The outflow boundary condition has been modelled according to an empirical pressure-flow relationship derived from reservoir properties [19,29]:

$$\tilde{A} + \tilde{B} \times M + \tilde{C} \times M^2 = P_{BHF}^2 - P_{res}^2 \qquad (40)$$

where, $\tilde{A}$ (Pa) is the minimum pressure required for the flow to start from the well into the reservoir, $\tilde{B}$ $(Pa.s/kg)$ and $\tilde{C}$ $(Pa.s/kg^2)$ are site-specific dimensional constants, M (kg/s) is the instantaneous mass flow rate at the bottom hole. P_{BHF}, (bar) and P_{res} (bar) are the instantaneous bottom hole pressure, and the reservoir static pressure respectively.

3.6 Heat exchange with the well layers

To reflect reality, eleven outer well layers are taken into account for the 1D radial heat transfer calculations (equations (10) to (12)). These include the tubing, A-annulus water, production casing, oil-based mud, surface casing, B-annulus water, cement, conductor casing, mudstone, sandstone, and chalk. The various layers are discretised into a number of

points in the radial direction from the well axis, and at every point the numerical finite volume heat transfer model computes the instantaneous temperature. Two boundary conditions, namely at the wall where the first well layer is in contact with the CO_2 mixture, and that for the outer layer in contact with the surrounding formation are employed. For the inner wall, the heat flux presented by equation (11) is prescribed for the outer wall. The formation temperature is assumed to be known from geological surveys.

4. Results and discussion

Given the availability of pertinent data for modelling purposes, the abandoned Peterhead CCS project [29] is used as a case study in this work. The project would have involved capturing one million tonnes of CO_2 per annum for 15 years from an existing combined cycle gas turbine located at Peterhead power station in Aberdeenshire, Scotland followed by pipeline transportation and injection into the depleted Golden Eye Reservoir. However, given the decision of the UK Government to withdraw the capital budget for the Carbon Capture and Storage Competition [51], the project was cancelled.

The data used for the case study include the well depth and geometry, pressure and temperature profiles, along with the surrounding formation characteristics as presented in [19,29] and summarised in Table 1.

Table 1: Main CO_2 injection simulation parameters

Parameter	Value
Well length	2582 m
Well internal diameter	0 – 800m depth: 0.125m 800 – 2582m depth: 0.0625m
Upstream pressure	115 bar
Inlet mass flow rate	Case 1: linearly ramped-up to 33.5 kg/s in 5 min Case 2: linearly ramped-up to 33.5 kg/s in 30 min Case 3: linearly ramped-up to 33.5 kg/s in 2 h
Upstream temperature	Case A: 278.15 K Case B: 283.15 K
Formation temperature	Varying linearly with depth from 277.15 K to 353.15 K along the well

4.1 Case studies

Six CO_2 injection scenarios are considered in this part of the study and the resulting transient pressure and temperature profiles along the well are simulated using the above model. The injection scenarios include linear ramping up to a maximum injection flow rate of 33.5 kg/s in 5 minmin (case 1), 30 min (case 2) and 2 h (case 3) each at two starting injection temperatures of 278.15 K (case A) and 283.15 K (case B) for the vertical well. For reference purposes, each of the six scenarios will be named after the corresponding ramping up scenario and temperature given in Table 1. For example, case 1-A refers to linear ramp-up from 0 to 33.5 kg/s in 5 min at a feed temperature of 278.15 K and so on.

To ensure numerical stability and convergence, a Courant–Friedrichs–Lewy condition of 0.3 [52] a relaxation time of 10^{-4}s and 300 computational cells are employed for conducting the injection simulations. For the numerical approximation of the heat exchanges with the well layers, the discretisation parameters given by [19] are employed. The above corresponds to ca ± 0.1% convergence error in the predicted temperatures and pressures.

For the heat transfer analysis, thickness, heat capacity, heat conductivity, and density for the eleven well layers are taken from [19]. To achieve converged solution of the heat conduction equation (12), the eight layers of well tubing and casing (overall thickness of ca 716 mm) have been discretised into 716 points, while 60 m of rock surrounding the well has been discretised into 1000 nodes.

The injection model was coded in FORTRAN, compiled using Intel compiler on Linux platform, and run on a desktop Intel® Xeon® W-2123 computer with 3.6 GHz CPU and 5Gb RAM.

The initial pressure and temperature profiles along the tapered well are given in Figures 3 and 4 respectively. The relatively low pressure at the bottom of the well (ca. 38 bar) means that the CO_2 remains in the gaseous phase in the first 400 m along the well, following which transition to the dense or liquid phase takes place (as indicated by the vertical dashed lines).

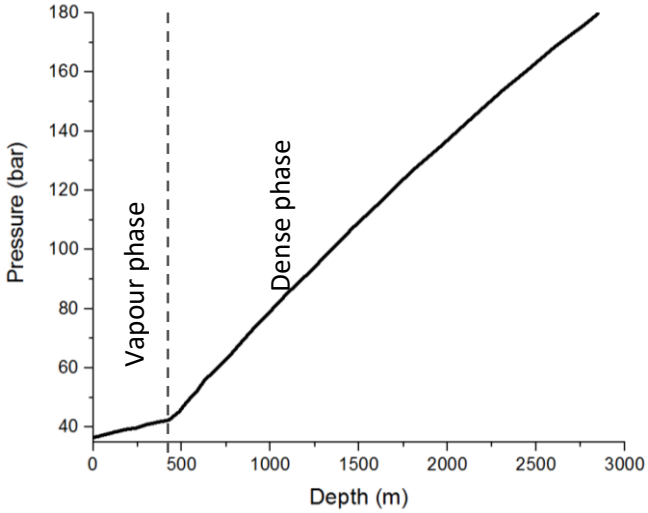

Figure 3: The initial pressure profile along the well (origin corresponds to the top of the well).

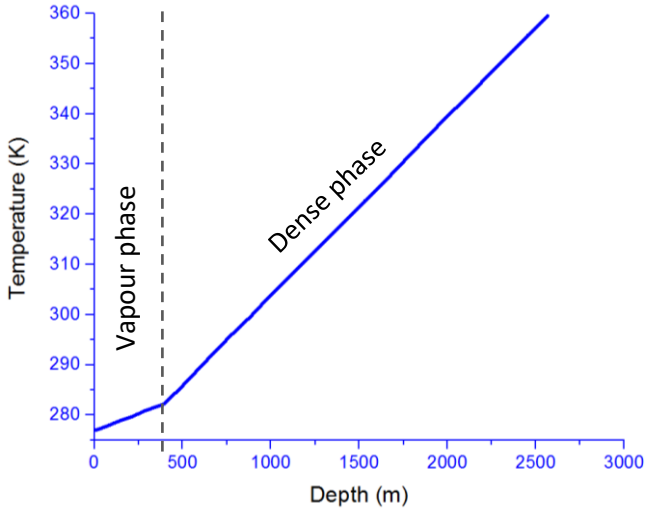

Figure 4: The initial temperature profile along the well (origin corresponds to the top of the well).

Figure 5 shows the variations of the CO_2 pressure and temperature at the top of the well as a function of time during the linear ramping up injection from 0 to 33.5 kg/s over min 300 s (case 1A). The feed CO_2 stream pressure and temperature are 115 bar and 278.15 K respectively. Figure 6 shows the same transient profiles but for the higher feed temperature of 283.15 K (case 1B) representing its prior heating. For both of the above initial conditions, the injected CO_2 is in the dense phase and remains so for the entire time frame (500 s) under consideration.

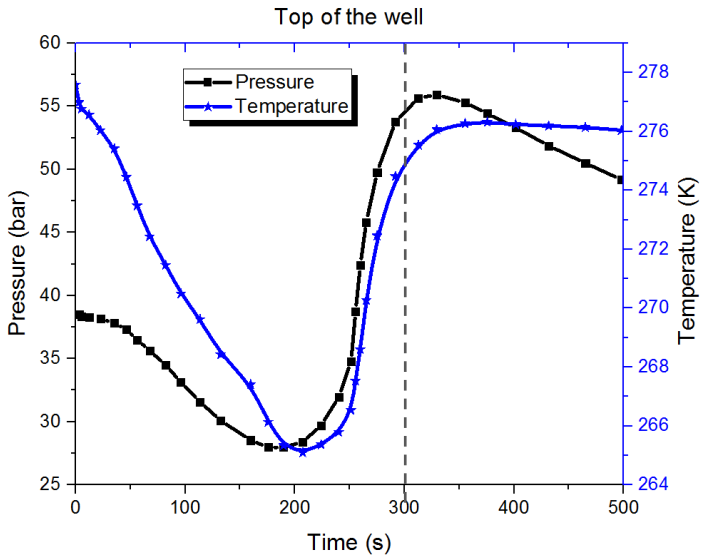

Figure 5: Transient pressure and temperature profiles at the top of the well for the fast injection ramping rate, case 1A (feed temperature 278.15 K). The vertical dashed line indicates the time (300 s) at which the injection flow rate reaches its peak value of 33.5 kg/s.

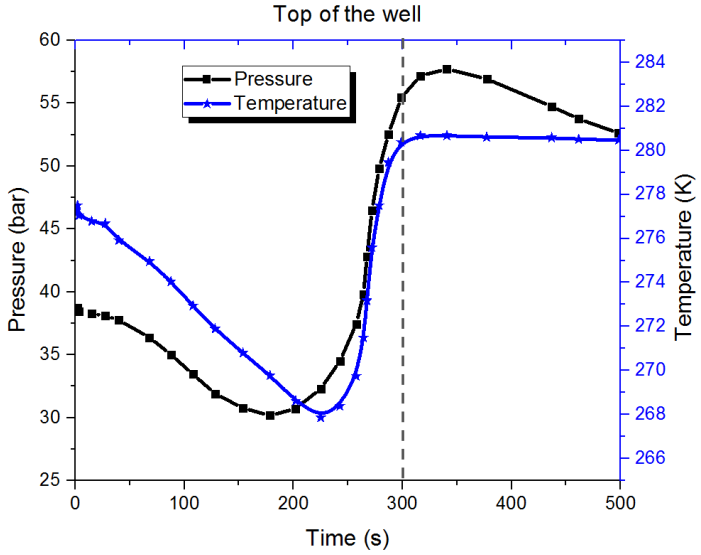

Figure 6: Transient pressure and temperature profiles at the wellhead for the fast injection ramping rate; case 1B (feed temperature 283.15 K). The vertical dashed line indicates the time (300 s) at which the injection flow rate reaches its peak value of 33.5 kg/s.

As it may be observed, in both cases an initial rapid depressurisation and cooling is followed by more rapid recoveries with the maximum values occurring at or shortly after the time (300 s) at which the injection rate reaches its peak value (33.5 kg/s). Also, whilst the temperature remains relatively constant thereafter, a secondary modest (ca. 5 bar) drop in the fluid pressure is obtained. As expected, the lower the feed temperature, the lower the minimum temperature attained. In the case of the feed temperature of 278.15 K, the lowest temperature reached at the top of the well is 265 K (case 1A). This compares with the slightly higher minimum temperature of 267.5 K for the feed temperature of 283.15 K (case 1B). Given that both of these minimum temperatures are below the freezing point for water, the presence of an appreciable amount of water in either the CO_2 stream or the well would pose the risk of blockage due to ice formation at the wellhead some 180 s after the injection process has commenced.

Figure 7 shows the CO_2 hydrate phase diagram [53]. The dark grey region (V-I-H) represents the conditions at which CO_2 hydrate is stable together with gaseous CO_2 and water ice (below 273.15 K). Table 2 shows the minimum CO_2 temperatures at the wellhead and the corresponding pressures for the six test scenarios (see Table 1).

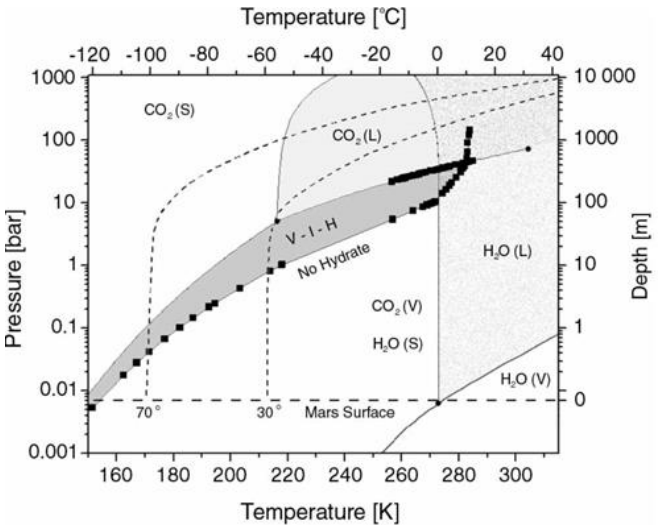

Figure 7: CO2 hydrate phase diagram [53] *
*permission to reproduce has been granted by the author.

Table 2: Lowest wellhead pressures and temperatures predicted for the examined cases

Simulation case	Inlet Temp (K)	Time at peak flow rate (s)	Lowest wellhead pressure (bar)	Lowest wellhead Temp (K)
1A	278.15	300	28	265
1B	283.15	300	30	267.5
2A	278.15	1800	24	258.5
2B	283.15	1800	26.5	261.5
3A	278.15	7200	20.5	252
3B	283.15	7200	22	256

Reference to Figure 7 along with the data presented in Table 2 indicates that hydrate formation is unlikely at the prevailing injection conditions.

Figure 8 and 9 respectively present the wellhead pressure and temperature transient profiles for the longer injection ramping up durations of 30 min (1800 s) and 2 h (7200 s). The feed temperature in both cases is 278.15 K (cases 2A and 3A). The observed trends in pressure and temperature are similar to those for the shorter ramping-up period with the exception of being more in concert with one another as compared to the faster pressure ramping scenarios. The latter is consistent with the longer opportunity for CO_2 to attain thermal and pressure equilibration along the injection well. For the medium injection rate (Figure 8), the termination of the temperature recoveries closely coincides with the time at which the peak injection rate is reached. In the case of the long injection rate however, thermal stabilisation occurs some 1800 s later. Most importantly, the longer the injection ramping up period, the lower is the minimum CO_2 temperature reached at the wellhead thus increasing the risk of wellhead blockage due to ice formation. The minimum temperature of ca. 252 K (21ºC below the freezing point for water) is observed for case 3-A (Figure 9) corresponding to an injection ramping-up period and temperature of 7200 s and 278.15 K respectively.

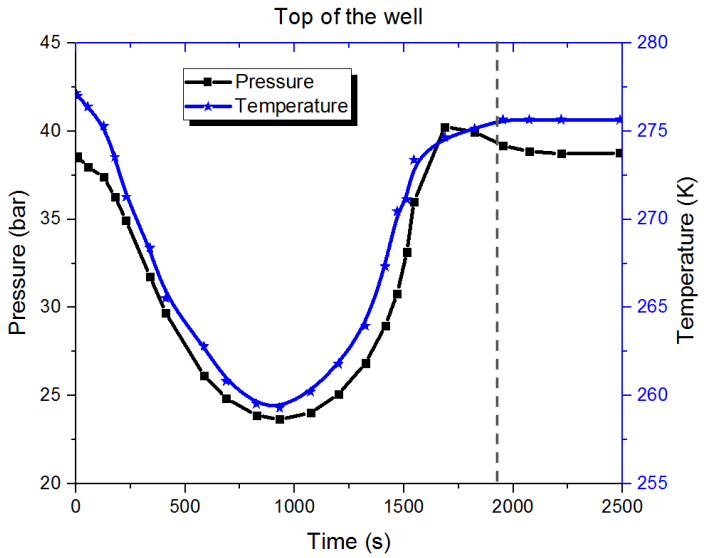

Figure 8: Transient pressure and temperature profiles at the top of the well for the medium injection ramping rate, case 2-A (feed temperature = 278.15 K). The vertical dashed line indicates the time (1800 s) at which the injection flow rate reaches its peak value of 33.5 kg/s.

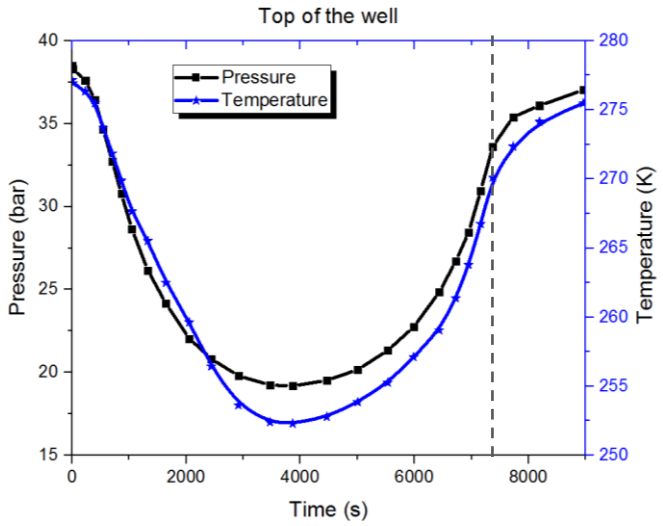

Figure 9: Transient pressure and temperature profiles at the top of the well for the slow injection ramping rate, case 3-A (feed temperature = 278.15 K). The vertical dashed line indicates the time (7200 s) at which the injection flow rate reaches its peak value of 33.5 kg/s.

Interestingly, as well as being more pronounced in the magnitude of their drops, the pressure and temperature profiles of cases 2-A (Figure 8) and 3-A (Figure 9) are in better concert with one another as compared to the faster pressure ramping scenarios (Figures 5 and 6). Also, for case 3-A (Figure 9) at 7200 s, where the linear ramp-up injection reaches the peak flow rate, neither the pressure nor the temperature immediately stabilise.

Figures 10 to Figure 12 respectively represent the variations of pressure and temperature at the bottom of the well as a function of time for the fast (Figure 10; case 1-A), medium (Figure 11: case 2-A) and slow (Figure 12: case 3-A) injection ramping strategies. The lower feed temperature of 278.15 K is assumed in all cases. As expected, the bottom well pressure increases as the CO_2 injection proceeds reaching a maximum value ca. 197 bar. Interestingly, for the medium (Figure 11) and the slow-injection ramping rates (Figure 12), the well bottom pressure reaches its maximum constant value at or soon after the time at which the peak injection rates are attained (1800 s and 7200 s). However in the case of the fast injection ramping up (Figure 10), the pressure at the bottom of the well keeps increasing, albeit by a modest amount, well after the maximum injection rate has been reached.

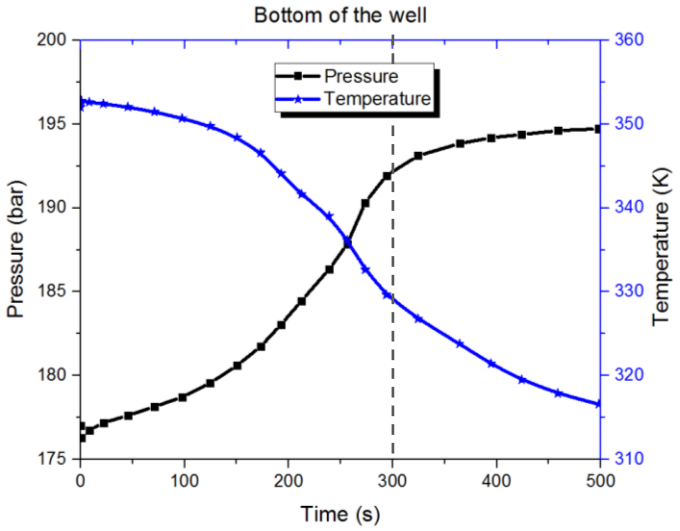

Figure 10: Transient pressure and temperature profiles at the bottom of the well for the fast injection ramping rate, case 1A (feed temperature 278.15 K; see

Table 1). The vertical dashed line indicates the time (300 s) at which the injection flow rate reaches its peak value of 33.5 kg/s.

Referring to the temperature profiles, in all three cases, the bottom well temperature decreases with time as the 'cooled' injected CO_2 at the top of the well travels towards it. Moreover, the magnitude of the drop in the temperature at the bottom of the well increases with increase in the injection ramping up period with the minimum temperature corresponding to 284.5 K. Given that this temperature is well above the freezing point for water, for the conditions simulated, there is no risk of ice or hydrate formation at the bottom of the well.

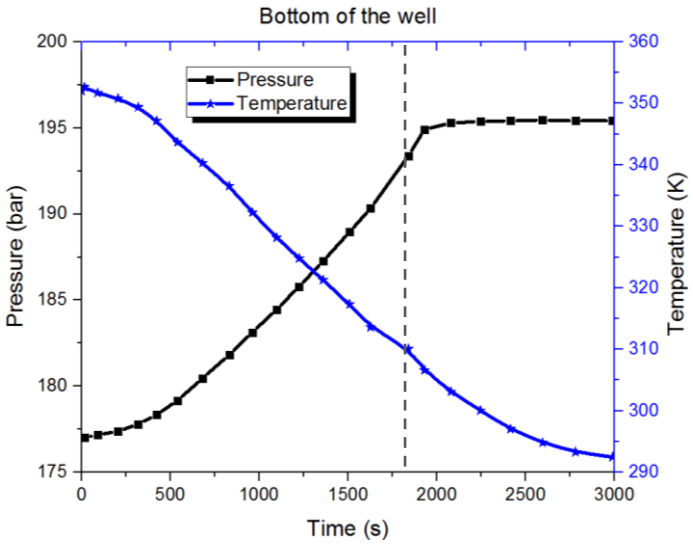

Figure 11: Transient pressure and temperature profiles at the bottom of the well for the medium injection ramping rate, case 2-A (feed temperature = 278.15 K). The vertical dashed line indicates the time (1800 s) at which the injection flow rate reaches its peak value of 33.5 kg/s.

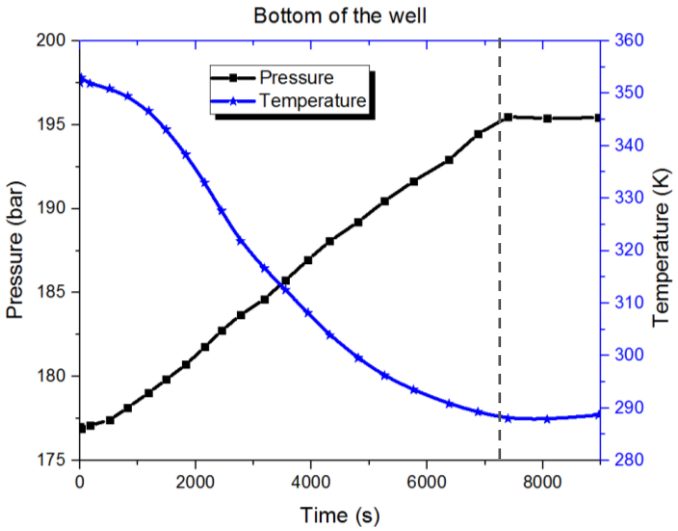

Figure 12: Transient pressure and temperature profiles at the bottom of the well for the slow injection ramping rate, case 3-A (feed temperature = 278.15 K). The vertical dashed line indicates the time (7200 s) at which the injection flow rate reaches its peak value of 33.5 kg/s.

Finally Figure 13 shows a comparison of the simulated wellhead transient temperature profiles at the three injection ramping up durations of 5 min (300 s), 30 min (1800 s) and 2 h (7200 s). The injection temperature and pressure are 276 K and 115 bar respectively. The solid lines represent the simulated data generated using the present model. The dotted lines on the other hand show the predicted data reproduced from the Peterhead CCS project report [29] for CO_2 injection into the depleted Golden Eye Reservoir using the commercial software, OLGA [26].

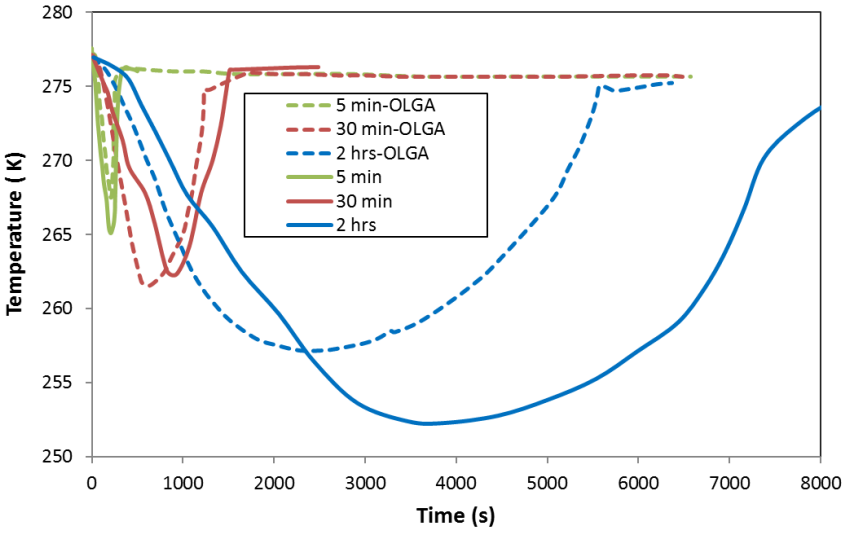

Figure 13. A comparison of the present model's predictions for the well head temperature for the three ramping up injection rates against those obtained using the commercial software, OLGA [26].

As it may be observed, both sets of simulations produce very similar trends; the initial rapid drop in temperature upon the injection of CO_2 is followed by a rapid recovery. The magnitude and the duration of the drop in temperature both increase with increase in the injection ramping up duration. Also, the slower the injection ramping up rate, the longer it takes for the fluid temperature to recover. Remarkably all three injection ramping up rates indicate minimum temperatures falling well below zero ^{o}C indicating the risk of well blockage due to ice formation in the event of the presence of appreciable amounts of water as well as the possibility of well bore fracture due to thermal shocking. This risk increases as the injection ramping up rate increases. As for the finite disagreement between the predictions between the two sets of simulations, it is difficult to draw any plausible conclusions given the absence of the detailed pertaining theory, in particular the formulation of the boundary conditions at the wellhead and the reservoir along with their implementation into the flow model capable of handling a time variant feed rate in the OLGA software.

5. Conclusion

As part of the challenge in combating global warming, depleted gas fields present ideal locations for storing the huge quantities of CO_2 captured from fossil fuel power plants and various energy intensive industrial emitters.

A significant expansion induced cooling of the high pressure CO_2 arriving at the top of the low pressure wellhead leading to the storage reservoir poses a number of potential hazards, including; well blockage, thermal shocking of the well bore steel lining and a reduction in the effective storage capacity. As such, the controlled gradual expansion of the CO_2 at the point of injection into the well balancing the requirement to minimise the temperature trop whilst ensuring maximum injection rate during the start-up injection is fundamentally important.

In this paper, we presented the development, testing and verification of a rigorous mathematical model for simulating the highly transient flow and heat transfer effects taking place throughout the well bore during the start-up injection of CO_2 into highly depleted gas reservoirs.

Through the development and integration of the appropriate boundary conditions at the wellhead, the well bottom (reservoir permeability) and taking into account the detailed well bore properties such as its heat transfer characteristics and the surrounding core, well tapering and deviation from the horizontal, our model can be used as useful practical engineering tool for determining the optimum injection ramping up rates.

Based on the application of the injection model simulating the injection of CO_2 in a real offshore depleted gas field in the North Sea, we make the following important observations for three selected nominal injection ramping up rates representing slow, medium and slow injection scenarios;

i) in all cases tested, the temperature of expanded CO_2 at the wellhead drops well below zero ^oC representing the risk of well blockage due to ice formation in the event of the presence of an appreciable amount of water and well bore fracture due to thermal shocking. However, well blockage due to hydrate formation proved unlikely;

ii) remarkably, the magnitude of the temperature drop increases with decrease in the injection ramping up rate. This means that slower injection ramping up rate gives rise to a higher risk of well blockage. The above observation is consistent with the published literature;

iii) as expected the preheating of the CO_2 prior to its injection reduces the risk of ice formation. However, the corresponding energy and hence cost implications will most likely not make this a viable option especially given the significant quantities of CO_2 being injected in practice (typically, millions of tonnes to reach full reservoir capacity);

iv) in none of the three test cases examined does the well bottom temperature drops below zero ^oC indicating minimal risk of the blockage of the well bore bottom perforations.

In conclusion, it is important to point out that the above observations are based on the application of the model developed to the particular, albeit realistic test case examined in the present study. As such the findings should not be considered as universally applicable to all cases involving injection of CO_2 into depleted gas reservoirs. Each injection scenario should be investigated based on the prevailing conditions. Certainly, this study shows that the choice of the injection ramping up rate has a profound impact on the highly transient temperature and pressure profiles incurring during the start-up injection process and the subsequent risks. The mathematical model presented in this work, once translated into a robust computational software, can be used as a valuable tool by engineers to determine the optimum injection ramping up rates into depleted gas reservoirs. This will contribute to accelerating the role out of CCS in transitioning the CO_2 emitting energy intensive industries onto a pathway consistent with the quest to limit the increase in the global average temperatures.

6. Acknowledgement

The authors are grateful to the UK Carbon Capture and Storage Research Centre for the funding of this work through the Flexible funding Call 2 C2-183.

7. NomenclatureA= well bore cross sectional Area (m^2)

$\tilde{A}$ = minimum pressure required for the flow to start from the well into the reservoir (Pa)

$\tilde{B}$ = site-specific dimensional constant (Pa s Kg^{-1})

$\tilde{C}$ = site-specific dimensional constant (Pa s Kg^{-2})

c_p = heat capacity at constant pressure (J K^{-1})

D_p = internal diameter of the pipe (m)

E = specific total energy (J Kg^{-1})

e = specific internal energy (J Kg^{-1})

F = viscous friction force

f_w = Fanning friction factor

g = gravitational acceleration (m s^{-2})

H = total enthalpy of the fluid (kJ kg^{-1})

k= fluid thermal conductivity (W m^{-1} K^{-1})

κ = heat conductivity (W m^{-1} K^{-1})

M = instantaneous mass flow rate at the bottom hole (kg s^{-1})

ml = meta-stable(super-heated) liquid phase

$\dot{m}$ = area-weighted mass flux (kg s^{-1} m^{-2})

$\mathcal{M}$= Mach number

$\bar{M}$= arithmetic averages of the values attained by Mach number

P= Mixture pressure (bar)

P_{BHF} = instantaneous bottom hole pressure (bar)

P_c = critical pressure (bar)

Pr = Fluid Prandtl number

P_{res} = reservoir static pressure (bar)

Re = Reynolds number

Q = heat flux (W m^{-2})

sv = saturated vapour phase

T= fluid temperature (K)

t = time (s)

T_c = critical temperature (K)

T_w = wall temperature (K)

u = mixture velocity (m s^{-1})

x = mixture vapour quality

z = space coordinate

Greek Symbols

ρ = mixture density (Kg m^{-3})

θ = relaxation time (s)

θ = well deviation from the vertical (º)

η = Corresponding heat transfer coefficient (W m^{-2} K^{-1})

ω = acentric factor for CO_2.

$\bar{\rho}$ = density of sound in cells i and $i+1$ (Kg m^{-3})

$\bar{a}$ = Speed of sound in cells i and $i+$ (m s^{-1})

8. References

[1] Energy Technology Perspectives 2017 https://webstore.iea.org/energy-technology-perspectives-2017

[2] Pale Blue Dot Energy. Progressing development of the UK's Strategic Carbon Dioxide Storage Resource: A Summary of Results from the Strategic UK CO2 Storage Appraisal Project 2016.

[3] Hughes DS. Carbon storage in depleted gas fields: Key challenges. Energy Procedia 2009;1:3007–14. doi:10.1016/j.egypro.2009.02.078.

[4] Sanchez Fernandez E, Naylor M, Lucquiaud M, Wetenhall B, Aghajani H, Race J, et al. Impacts of geological store uncertainties on the design and operation of flexible CCS offshore pipeline infrastructure. Int J Greenh Gas Control 2016;52:139–54. doi:10.1016/j.ijggc.2016.06.005.

[5] ETI. Reducing the cost of CCS developments in capture plant technology. 2016.

[6] Eiken O, Ringrose P, Hermanrud C, Nazarian B, Torp TA, Høier L. Lessons Learned from 14 years of CCS Operations: Sleipner, In Salah and Snøhvit. Energy Procedia 2011;4:5541–8. doi:10.1016/j.egypro.2011.02.541.

[7] Jiang P, Li X, Xu R, Wang Y, Chen M, Wang H, et al. Thermal modeling of CO2 in the injection well and reservoir at the Ordos CCS demonstration project, China. Int J Greenh Gas Control 2014;23:135–46. doi:10.1016/j.ijggc.2014.01.011.

[8] Shell Canada Limited. Quest Carbon Capture and Storage Project 2017.

[9] Böser W, Belfroid S. Flow Assurance Study. Energy Procedia 2013;37:3018–30. doi:10.1016/j.egypro.2013.06.188.

[10] Mahgerefteh H, Oke AO, Rykov Y. Efficient numerical solution for highly transient flows. Chem Eng Sci 2006;61:5049–56. doi:10.1016/j.ces.2006.03.012.

[11] Mahgerefteh H, Brown S, Denton G. Modelling the impact of stream impurities on ductile fractures in CO2 pipelines. Chem Eng Sci 2012;74:200–10. doi:10.1016/j.ces.2012.02.037.

[12] Brown S, Martynov S, Mahgerefteh H, Chen S, Zhang Y. Modelling the non-equilibrium two-phase flow during depressurisation of CO2 pipelines. Int J Greenh Gas Control 2014;In review:9–18.

doi:10.1016/j.ijggc.2014.08.013.
[13] Oldenburg CM. Joule-Thomson cooling due to CO2 injection into natural gas reservoirs. Energy Convers Manag 2007;48:1808–15. doi:10.1016/j.enconman.2007.01.010.
[14] André L, Audigane P, Azaroual M, Menjoz A. Numerical modeling of fluid-rock chemical interactions at the supercritical CO2-liquid interface during CO2 injection into a carbonate reservoir, the Dogger aquifer (Paris Basin, France). Energy Convers Manag 2007;48:1782–97. doi:10.1016/j.enconman.2007.01.006.
[15] Oldenburg CM, Moridis GJ, Spycher N, Pruess K. EOS7C Version 1.0: TOUGH2 Module for Carbon Dioxide or Nitrogen inNatural Gas (Methane) Reservoirs. Berkeley, CA: 2004. doi:10.2172/878525.
[16] Goodarzi S, Settari A, Zoback MD, Keith D. Thermal Aspects of Geomechanics and Induced Fracturing in CO2 Injection With Application to CO2 Sequestration in Ohio River Valley. SPE Int Conf CO2 Capture, Storage, Util 2010;2. doi:10.2118/139706-MS.
[17] Linga G, Lund H. A two-fluid model for vertical flow applied to CO2 injection wells. Int J Greenh Gas Control 2016;51:71–80. doi:10.1016/j.ijggc.2016.05.009.
[18] Span R, Wagner W. A New Equation of State for Carbon Dioxide Covering the Fluid Region from the Triple-Point Temperature to 1100 K at Pressures up to 800 MPa. J Phys Chem Ref Data 1996;25:1509. doi:10.1063/1.555991.
[19] Li X, Xu R, Wei L, Jiang P. Modeling of wellbore dynamics of a CO2 injector during transient well shut-in and start-up operations. Int J Greenh Gas Control 2015;42:602–14. doi:10.1016/j.ijggc.2015.09.016.
[20] Lu M, Connell LD. Non-isothermal flow of carbon dioxide in injection wells during geological storage. Int J Greenh Gas Control 2008;2:248–58. doi:10.1016/S1750-5836(07)00114-4.
[21] Paterson L, Lu M, Connell L, Ennis-King J. Numerical Modeling of Pressure and Temperature Profiles Including Phase Transitions in Carbon Dioxide Wells. SPE Annu Tech Conf Exhib Denver, Color USA, Sept 21-24 2008. doi:10.2118/115946-MS.
[22] Lindeberg E. Modelling pressure and temperature profile in a CO2 injection well. Energy Procedia 2011;4:3935–41. doi:10.1016/j.egypro.2011.02.332.
[23] Pan L, Webb SW, Oldenburg CM. Analytical solution for two-phase flow in a wellbore using the drift-flux model. Adv Water Resour 2011;34:1656–65. doi:10.1016/j.advwatres.2011.08.009.
[24] Lu M, Connell LD. The transient behaviour of CO2 flow with phase transition in injection wells during geological storage – Application to a case study. J Pet Sci Eng 2014;124:7–18. doi:10.1016/j.petrol.2014.09.024.
[25] Tollak S, Bernstone C, Clausen S, Koeijer G De, Mølnvik MJ. Combining thermodynamic and fluid flow modelling for CO 2 flow assurance 2013;00.
[26] Bendiksen KH, Maines D, Moe R, Nuland S. The Dynamic Two-Fluid Model OLGA: Theory and Application. SPE Prod Eng 1991;6:171–80. doi:10.2118/19451-PA.
[27] Li X, Li G, Wang H, Tian S, Song X, Lu P, et al. International Journal of Greenhouse Gas Control A unified model for wellbore flow and heat transfer in pure CO 2 injection for geological sequestration , EOR and fracturing operations. Int J Greenh Gas Control 2017;57:102–15. doi:10.1016/j.ijggc.2016.11.030.
[28] Lund H, Torsæter M, Munkejord ST. Study of Thermal Variations in Wells During Carbon Dioxide Injection. Soc Pet Eng - SPE Bergen One Day Semin 2015 2015;31:327–37. doi:10.2118/173864-PA.
[29] Shell. Peterhead CCS Project. 2015.
[30] Lu M, Connell LD. Transient, thermal wellbore flow of multispecies carbon dioxide mixtures with phase transition during geological storage. Int J Multiph Flow 2014;63:82–92. doi:10.1016/j.ijmultiphaseflow.2014.04.002.
[31] Raza A, Gholami R, Rezaee R, Bing CH, Nagarajan R, Hamid MA. Well selection in depleted oil and gas fields for a safe CO2 storage practice: a case study from Malaysia. Petroleum 2016. doi:10.1016/j.petlm.2016.10.003.
[32] Brown S, Martynov S, Mahgerefteh H, Proust C. A homogeneous relaxation flow model for the full bore rupture of dense phase CO2 pipelines. Int J Greenh Gas Control 2013;17:349–56. doi:10.1016/j.ijggc.2013.05.020.
[33] Brown S, Martynov S, Mahgerefteh H. Simulation of two-phase flow through ducts with discontinuous cross-section. Comput Fluids 2015;120:46–56. doi:10.1016/j.compfluid.2015.07.018.
[34] Downar-Zapolski P, Bilicki Z, Bolle L, Franco J. The non-equilibrium relaxation model for one-dimensional flashing liquid flow. Int J Multiph Flow 1996;22:473–83. doi:10.1016/0301-9322(95)00078-X.
[35] Chen NH. An Explicit Equation for Friction Factor in Pipe. Ind Eng Chem Fundam 1979;18:296–7. doi:10.1021/i160071a019.
[36] Wood DA. Metaheuristic profiling to assess performance of hybrid evolutionary optimization algorithms applied to complex wellbore trajectories. J Nat Gas Sci Eng 2016;33:751–68. doi:10.1016/j.jngse.2016.05.041.
[37] Chabook M, Al-Ajmi A, Isaev V. The role of rock strength criteria in wellbore stability and trajectory optimization. Int J Rock Mech Min Sci 2015;80:373–8. doi:10.1016/j.ijrmms.2015.10.003.
[38] Dittus FW, Boelter LMK. Heat Transfer in Automobile Radiators 1930;2:443.

[39] Peng D-Y, Robinson DB. A New Two-Constant Equation of State. Ind Eng Chem Fundam 1976;15:59–64. doi:10.1021/i160057a011.
[40] Diamantonis NI, Economou IG. Evaluation of statistical associating fluid theory (SAFT) and perturbed chain-SAFT equations of state for the calculation of thermodynamic derivative properties of fluids related to carbon capture and sequestration. Energy and Fuels 2011;25:3334–43. doi:10.1021/ef200387p.
[41] Poling BE, Prausnitz JM, O'Connell JP. The properties of gases and liquids. McGraw-Hill; 2001.
[42] Liou MS. A sequel to AUSM, Part II: AUSM+-up for all speeds. J Comput Phys 2006;214:137–70. doi:10.1016/j.jcp.2005.09.020.
[43] Liou M. A Sequel to AUSM: AUSM. J Comput Phys 1996;129:364–82. doi:10.1006/jcph.1996.0256.
[44] Niu Y-Y, Lin Y-C, Chang C-H. A further work on multi-phase two-fluid approach for compressible multi-phase flows. Int J Numer Methods Fluids 2008;58:879–96.
[45] Paillère H, Corre C, García Cascales JR. On the extension of the AUSM+ scheme to compressible two-fluid models. Comput Fluids 2003;32:891–916. doi:10.1016/S0045-7930(02)00021-X.
[46] Robbins DJ, Cant RS, Gladden LF. Development of accurate, robust liquid equations of state for multi-phase CFD simulations with a modified AUSM+-up scheme. Comput Fluids 2013;77:166–80. doi:10.1016/j.compfluid.2013.01.031.
[47] Liou MM-S, Nguyen L, Theofanous TG, Chang CC-H, Nguyen L, Theofanous TG. How to Solve Compressible Multifluid Equations: a Simple, Robust, and Accurate Method. AIAA J 2008;46:2345–56. doi:10.2514/1.34793.
[48] LeVeque RJ. Finite Volume Methods for Hyperbolic Problems: Cambridge: Cambridge University Press; 2002. doi:10.1017/CBO9780511791253.
[49] Thompson KW. Time dependent boundary conditions for hyperbolic systems. J Comput Phys 1987;68:1–24. doi:10.1016/0021-9991(87)90041-6.
[50] Thompson KW. Time-dependent boundary conditions for hyperbolic systems, {II}. J Comput Phys 1990;89:439–61. doi:10.1016/0021-9991(90)90152-Q.
[51] Cotton A, Gray L, Maas W. Learnings from the Shell Peterhead CCS Project Front End Engineering Design. Energy Procedia 2017;114:5663–70. doi:10.1016/J.EGYPRO.2017.03.1705.
[52] Mahgerefteh H, Rykov Y, Denton G. Courant, Friedrichs and Lewy (CFL) impact on numerical convergence of highly transient flows. Chem Eng Sci 2009;64:4969–75. doi:10.1016/J.CES.2009.08.002.
[53] Genov GY. Physical processes of the CO2 hydrate formation and decomposition at conditions relevant to Mars 2005.

kgkg